Biomaterials 29 (2008) 2794–2801

Contents lists available at ScienceDirect

Biomaterials

journal homepage: www.elsevier.com/locate/biomaterials

A sandwich structured SiO_2/cytochrome *c*/SiO_2 on a boron-doped diamond film electrode as an electrochemical nitrite biosensor

Rong Geng, Guohua Zhao *, Meichuan Liu, Mingfang Li

Department of Chemistry, Tongji University, 1239 Siping Road, Shanghai 200092, People's Republic of China

ARTICLE INFO

Article history:
Received 16 January 2008
Accepted 4 March 2008
Available online 3 April 2008

Keywords:
Sandwich structured
Protein
Bioelectrocatalysis
Diamond
Nitrite

ABSTRACT

A novel sandwich structured SiO_2 gel/cytochrome *c* (Cyt *c*)/SiO_2 gel was designed and constructed on conductive boron-doped diamond (BDD) film substrate. A SiO_2 gel membrane was first *in situ* deposited on the pretreated positive charged H-terminated BDD electrode with a simple and artful surface vapor sol–gel method. Cyt *c* was subsequently immobilized onto the SiO_2 membranes by electrostatic attraction, followed by another SiO_2 gel layer *in situ* depositing on it. The SiO_2 interlayer was conceived to play an important role in the resultant sandwich structured SiO_2/Cyt *c*/SiO_2/BDD electrode as a selective "semi-open" medium, which guaranteed the immobilized Cyt *c* to maintain high stability and perform good electrochemistry and biocatalysis responses. The bioactivity of Cyt *c* was well protected and the immobilized biomolecule even didn't denature at extremely high or low pH condition. More attractively, Cyt *c* in the sandwich structured electrode could be further oxidized into highly reactive Cyt *c* π-cation by two-step electrochemical oxidation, which could oxidize NO_2^- into NO_3^- in the solution. A sensitive determination approach of nitrite was accordingly built up based on this biocatalytic oxidative interaction for the first time and a possible mechanism of the interaction was herein proposed.

1. Introduction

Cytochrome *c* (Cyt *c*) has drawn a lot of research interest due to its electrochemistry activity and the role of transferring electrons in respiration process [1]. It is also well accepted that Cyt *c* exhibits peroxidase activities, which can catalyze the reductive reaction of hydrogen peroxide. Determinations to H_2O_2 based on such catalytic interactions are widely reported [2,3]. Effective immobilization and maintenance to the bioactivity on a proper substrate are essential to get a stable and sensitive response signal. Many methods for protein immobilization are extensively investigated, such as physical methods [4,5]. However, decrease of signal resulting from high charge transfer resistance is unavoidable, meanwhile, the bioactivity and electroactivity are also restrained. Great efforts have been taken to covalent interaction technique, since it promises firmly immobilization and ordered orientation of biomolecule [6,7]. Therefore, most of the key-and-lock sensors developed nowadays employ covalent coupling. However, the activity of biomolecule is highly influenced by environment, such as temperature and pH. The covalent immobilized biomolecules are entirely exposed to the electrolyte in such "full-open" system, which makes the biomolecule denature and deactivate easily.

Embedded method [8,9] has the advantage of providing mild microenvironment to the trapped biomolecule, which helps to maintain its bioactivity and offers a possibility to extend the application of biodevices in complex conditions. Thus, more research interest has been drawn. Choice of matrix materials is crucial for embedded method, since it acts as not only the biomolecule carrier but also the electron transfer tunnel between the trapped biomolecule and substrate electrode. Ideal embedded material must be stretchy and moist, which mimics the biomembrane, and offers mild microenvironment for the inner biomolecule, such as lecithoid membrane. In view of this, a "semi-open" property is favored and essential, which permits the communication between inner biomolecule and outer environment, and protects the biomolecule from the influence of extreme environment simultaneously. Besides, the electron transfer must be ensured. SiO_2, as one kind of promising inorganic nanomembrane materials, has recently attracted much attention due to its many superior properties such as tunable porosity, high thermal stability, chemical inertness, and so on [10–13]. Novel structures, such as layer-by-layer [12] and core–shell [13], have been designed to increase the quantity of embedded biomolecules and maintain the bioactivity.

Substrate plays a leading role in the performance of modified electrode. A lot of biosensors based on conventional substrates, such as glass carbon [14] (GC), gold [15] and other materials, have been reported. However, disadvantages as low stability and inhibition are also found. Electrically conducting boron-doped diamond (BDD)

* Corresponding author. Tel.: +86 21 65 988 570; fax: +86 21 65 982 287.
E-mail address: g.zhao@mail.tongji.edu.cn (G. Zhao).

0142-9612/$ – see front matter © 2008 Elsevier Ltd. All rights reserved.
doi:10.1016/j.biomaterials.2008.03.004

thin-film exhibits many superior electrochemical properties [16–20], and it is widely considered to be biocompatible. Hence, the BDD electrodes attract much interest for electrochemical and biological applications, such as electroanalysis, electrosynthesis, electrochemical wastewater treatment, etc [21–27]. Application of BDD in electroanalysis is a brisk field and has been well summarized by Compton et al. [28], either on as-grown BDD or functionalized BDD, both in detecting biological samples [21,25,26] and organic pollutants [22–24,27], and so on. Good sensitivity and repeatability were obtained owing to its resistance to fouling. However, such inertness also makes BDD difficult to be modified. Therefore biosensors based on the substrate have not been abundantly reported.

In our present work, BDD electrode was chosen as the substrate. A sandwich structure was finally designed and constructed. The "semi-open" SiO_2 interlayer retained the bioactivity and electroactivity of Cyt *c*, and permitted good communication between inner Cyt *c* and outer bulk electrolyte simultaneously. Further more, biocatalytic oxidative property to nitrite was observed, and a possible mechanism was proposed. Our need and desire to monitor nitrite ion are unquestionable, yet their ubiquity can pose a significant challenge to the analytical community. Strategies were comprehensively surveyed by Moorcroft and coworkers [29]. Metal and metal oxide modified electrode have good catalytic properties to nitrite, either oxidative [30–32] or reductive [33,34]. Those sensors possess advantages including ease of construction, comparative detection limit, low cost, and so on. Nitrite biosensors [35–39] have been widely reported since many proteins are proven to catalyze the reductive reaction of nitrite. However, these biosensors are all attributed to the electroreductive reactions, which is complicated and the products are complex. Furthermore, many of them are conducted under weak acidic medium, in which dismutation will often happen and influence the detection a lot. Electrooxidative properties of Cyt *c* are seldom reported [40,41]. To our best knowledge, up till now, no electrochemical nitrite biosensors have been fabricated based on Cyt *c*, especially on the electro oxidative reactions, although it is indicated that there are interactions between Cyt *c* and nitrite [42–46]. Herein, a nitrite biosensor was designed based on the simple electro oxidative interaction with nitrate as the unique product for the first time. Satisfactory linear range and detection limit were obtained with good sensitivity.

2. Experimental

2.1. Materials

Horse heart cytochrome *c* (Cyt *c*, MW 12,384), was purchased from Sigma, and used as received. Tetraethyl orthosilicate (TEOS) was purchased from Sinopharm Chemical Reagent Co., Ltd (China). All other chemicals were of analytical reagent grade and used without further purification. $NaNO_2$ solution was freshly prepared. The supporting electrolyte was 25 mM phosphate buffer solution (PBS), which was prepared with KH_2PO_4 and Na_2HPO_4. The pH was adjusted with H_3PO_4 or NaOH. Acetate buffer solution (ABS, 0.2 M, pH 4.5) was prepared by mixing stock standard solutions of HAc and NaAc. All solutions were made up with twice-distilled water.

2.2. Construction of the sandwich and layer-by-layer structure

First, the BDD electrode of 15 mm^2 area was pretreated by cyclic voltammetry method between −3.0 and 0 V, 120 cycles in 1 M H_2SO_4 solution. Second, an aliquot of 10 μL ABS was dropped onto the pretreated surface. The electrode was suspended upside down above liquid TEOS in a sealed plastic tubule at required temperature and time. The SiO_2 sol–gel layer was formed through hydrolysis of TEOS vapor. Third, the electrode was washed and dried in air at ambient temperature. Then, it was immersed into a pH 6.86 PBS containing 1×10^{-4} M Cyt *c* for 30 min. Thus one bilayer was obtained. The second step was conducted once more to obtain a sandwich-like modified electrode, or the second and third steps were repeated for desired times to get a layer-by-layer modified electrode.

2.3. Characteristic study

Ultraviolet and visible (UV–vis) absorption spectra were recorded at the wavelength ranging from 190 to 1100 nm at room temperature using Aglient 8453 UV–vis spectrophotometer. SEM images were obtained on Quanta 200 FEG scanning electron microanalyzer (FEI Company, Japan), and AFM images on Benyuan CSPM-4000 (China) with a platinum cantilever operated in tapping mode. X-ray diffraction (XRD) was done with D8 Advance XRD spectra (Bruker Co., Ltd., Germany), using a CuKR source at 40 kV and 120 mA with a scan rate of 3°/min.

2.4. Electrochemical measurements

Electrochemical measurements were carried out on a CHI 660C electrochemistry working station (CH Instrument, USA). A conventional three-electrode cell was used with a saturated calomel electrode (SCE, Shanghai Precision and Scientific Instrument Co., Ltd, China) as the reference, a platinum wire as the counter, and a BDD or modified BDD electrode as the working electrode. Cyclic voltammetry (CV) and differential pulse voltammetry (DPV) were conducted in PBS, containing $NaNO_2$ with different concentrations. Electrochemical independence spectroscopy (EIS) was performed in 0.1 M KCl with 5.0 mM $K_3Fe(CN)_6/K_4Fe(CN)_6$ (1:1) mixture as electroactive probe, using an alternating voltage of 5.0 mV. The impedance measurements were recorded at a potential of 200 mV within the frequency range of 10^{-2}–10^5 Hz. Before each measurement, solutions were purged with purified nitrogen for at least 15 min, and a nitrogen environment was then maintained over the solutions during the experimental processes. All experiments were performed at ambient temperature.

3. Results and discussion

3.1. Design and construction of SiO_2/Cyt c/SiO_2 sandwich structure on BDD electrode

The construction process of sandwich structured SiO_2/Cyt *c*/SiO_2 on BDD electrode was shown in Scheme 1. A simple electrochemical cathodic method, that is, CV scanning between 0 and −3.0 V (vs SCE) for 120 cycles, was first developed to pretreat the BDD electrode, resulting in the H-terminated and positively charged BDD surface [47,48]. Compared with other substrates, it was much easier to functionalize the surface of BDD. For example, when GC [49] or pyrolytic graphite [50] (PG) was used, a precursor such as poly (diallyldimethylammonium) (PDDA) must be introduced to make the electrode surface positively charged.

Surface vapor sol–gel method evolved from Hu's previous report [51] was used here to generate SiO_2 gel onto the BDD surface, as shown in Scheme 1b and c. Compared to Hu's method, our procedure was much more time-saving. The main improvements lied in both the acidic condition of the hydrolysis medium and the temperature of TEOS.

Hydrolysis of TEOS may be a multiple process, but can be summarized as the following equation: $(CH_3CH_2O)_4Si + 2H_2O \rightarrow SiO_2 + 2C_2H_5OH$, which is usually catalyzed by strong acid or strong base. Here, pH 4.5 ABS was chosen as the hydrolysis reaction solution, which allowed a satisfactory TEOS hydrolysis rate, and wasn't harmful to the activity of Cyt *c*. Further more, the isoelectric point (pI) of SiO_2 is 2–3, which means the produced SiO_2 gel is negatively charged in pH 4.5 ABS and can firmly adhere to the positively charged BDD substrate.

Since the vapor pressure and hydrolysis activity of TEOS are influenced greatly by the temperature, increasing the temperature will be an effective way to accelerate the hydrolysis rate. It's very interesting and attractive that, Cyt *c* has very good thermal stability after immobilized into the SiO_2 gel. UV–vis study showed that the soret band of Cyt *c* in the SiO_2 gel didn't change even after thermal treated for 60 min at 100 °C. It might be because that the SiO_2 gel could hamper the unfolding of peptide chains and hence indicated a significant beneficial effect on the thermal stability of Cyt *c*. In virtue of this, a higher temperature could be adopted in surface vapor sol–gel process.

Influence of hydrolysis time and temperature of TEOS on the ability of trapping biomolecule and the activity as electron transfer medium to the SiO_2 gel was investigated. Experiment results got from direct electrochemistry under different conditions are listed in Table 1. It could be seen that the SiO_2 gel constructed at 50 °C,

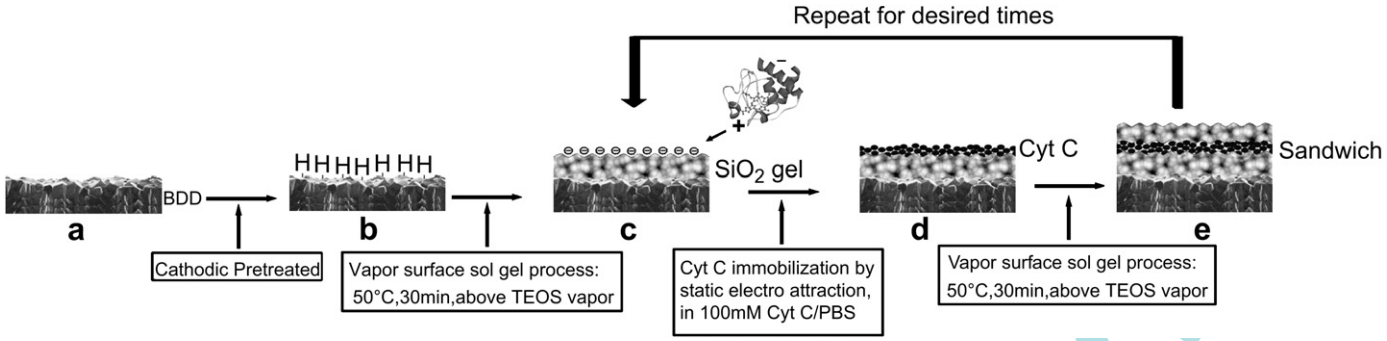

Scheme 1. The SiO_2/Cyt *c*/SiO_2 sandwich structure construction process on BDD.

30 min acted as the best electron transfer tunnel. This was mainly due to the different thickness as a result of different construction conditions. At low temperature, when time was short, the SiO_2 gel layer was too thin to cover the substrate or offer enough adsorption position to Cyt *c*. However, when hydrolysis time was too long at high temperature, the gel became so thick that even blocked the electron transfer between Cyt *c* and the substrate. Therefore, 50 °C and 30 min were chosen as the optimized temperature and time, respectively.

Immobilization of Cyt *c* was realized by self-assembly in Cyt *c*/PBS (pH 6.86), as shown in Scheme 1c and d. The pI of Cyt *c* was 10.5, which indicated that the Cyt *c* molecule was positively charged in the neutral medium. Therefore, Cyt *c* could be trapped in the SiO_2 gel layer by electrostatic attraction since the fabricated SiO_2 gel was negatively charged in the same medium. Results of the direct electrochemistry showed that 30 min was enough to get a saturated adsorption of Cyt *c* and also the maximum direct electrochemistry response. As clearly shown in Scheme 1, the orientation of the immobilized Cyt *c* molecule was characterized by the positively charged part pointed to the substrate electrode, due to unequal charge distribution on the surface of the molecule, which would also improve the direct electrochemistry of biomolecule dramatically.

Layer-by-layer method is widely used to increase the quantity of immobilized biomolecule in order to improve electrochemistry signal. In the present study, surface vapor sol–gel and adsorption steps were repeated for desired times and accordingly the layer-by-layer structure was obtained, signified as (Cyt *c*/SiO_2)$_n$, *n* stands for the number of (Cyt *c*/SiO_2) bilayers.

As illustrated in Fig. 1, the redox peak currents decreased with increasing *n*. (Cyt *c*/SiO_2)$_1$ showed well shaped redox peaks (Fig. 1a, curve 1), but the peak current decreased a lot for (Cyt *c*/SiO_2)$_5$ (Fig. 1a, curve 2). As to (Cyt *c*/SiO_2)$_{12}$, the redox peaks even could not be defined (Fig. 1a, curve 3). It implied that the quantity of electroactive Cyt *c* could not be increased by increasing the number of the bilayers. In other words, the electroactivity of Cyt *c* was greatly influenced by the distance between biomolecules and substrate, or the thickness of SiO_2 gel.

Table 1
The influence of deposited time and temperature on the direct electrochemistry of immobilized Cyt *c*

T/°C	Time/min	Formal potential/V	I_{pa}/μA	I_{pc}/μA
30	30	–	–	−4.958
	60	−0.072	55.08	−85.84
	90	−0.035	11.98	−17.80
	120	0	8.78	−10.02
40	30	−0.069	39.45	−49.10
	60	0.016	27.02	−38.39
	90	–	–	−5.960
	120	–	–	−7.580
50	30	−0.075	68.09	−90.07
	60	0.026	18.62	−29.75
	90	–	–	–
	120	–	–	–

Formal potential, oxidation current (I_{pa}) and reduction current (I_{pc}) are listed; (–) means no direct electrochemistry signal was detected.

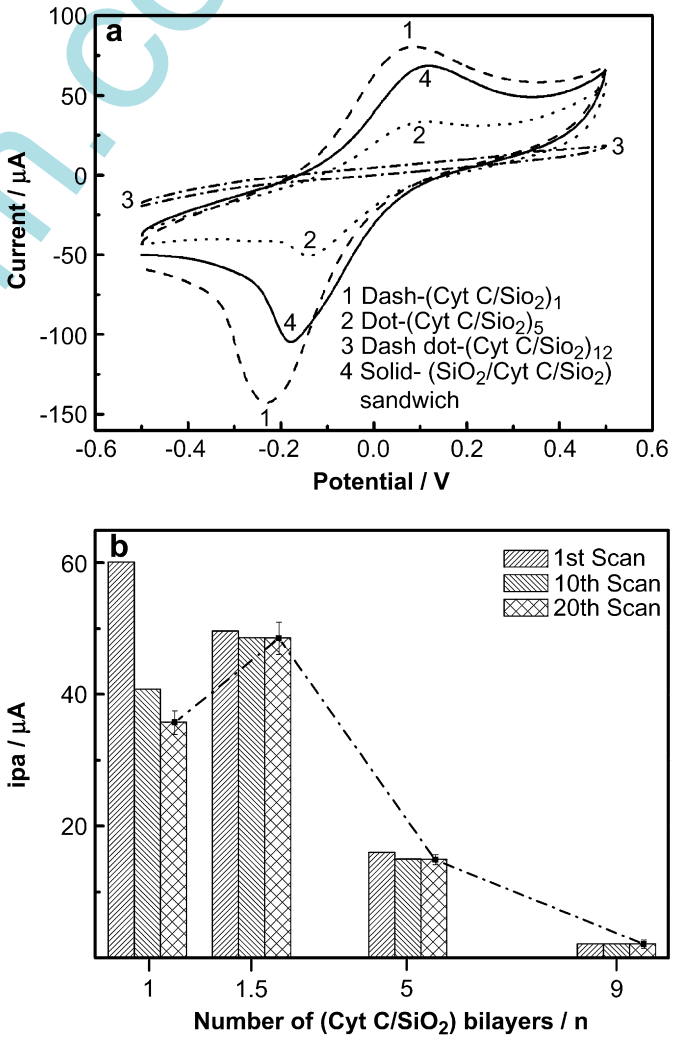

Fig. 1. (a) CVs of (Cyt *c*/SiO_2)$_n$ (*n* = 1, 1.5, 5 and 12, respectively)/BDD electrode in PBS (first scan, scan rate 0.1 V/s); (b) relationship between anodic peak current I_{pa} of (Cyt *c*/SiO_2)$_n$/BDD electrode with scan times (1st, 10th and 20th cycles) and layer number *n* (*n* = 1, 1.5 and 5, respectively).

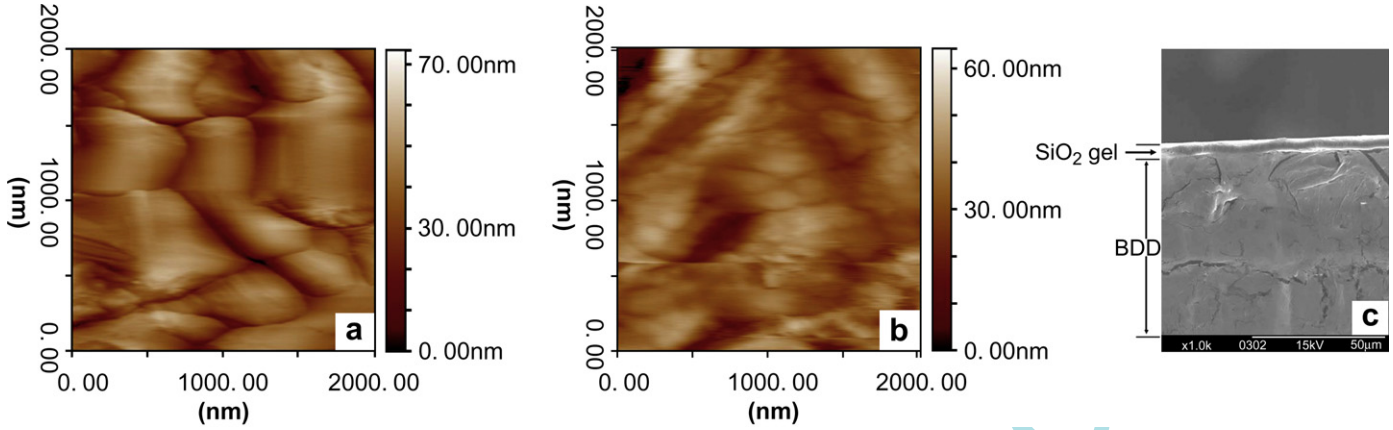

Fig. 2. The AFM images of SiO_2/BDD (a), Cyt *c*/SiO_2/BDD (b) and the SEM image of SiO_2/BDD profile (c) fabricated at optimized condition.

Nevertheless, as shown in Fig. 1b, opposite to the peak current, stability of the modified electrode, which was estimated by the peak current value variation after successive scanning in PBS, improved obviously with increasing the number of bilayers. That is to say, peak current of (Cyt *c*/SiO_2)$_1$/BDD decreased greatly with the numbers of CV scan, but as to (Cyt *c*/SiO_2)$_n$/BDD ($n > 1$), this disadvantage was restrained. Since the stable current reached the maximum value when n was 1.5 (as shown in dotted curve in Fig. 1b), a sandwich-like framework, SiO_2/Cyt *c*/SiO_2 structure ($n = 1.5$) was thereafter constructed and chosen to be the optimized case to obtain sensitive electrochemistry response and good stability. Although the peak current in the first scan decreased a little compared to (Cyt *c*/SiO_2)$_1$/BDD, the peak shape almost didn't change in successive CV scans (Fig. 1a, curve 4). When a stable CV curve was obtained (about 20 scans), direct electrochemistry of sandwich/BDD was much better than (Cyt *c*/SiO_2)$_1$/BDD. The result proved that the electroactivity of Cyt *c* could be well displayed in the sandwich, and the outer gel layer effectively prevented immobilized Cyt *c* from desorption.

3.2. Characterization of SiO_2/Cyt *c*/SiO_2 sandwich structure

Micromorphology of the modified electrodes was investigated by AFM and SEM. The fluctuation of the electrodes surfaces, which was closely related to the structure, scale and formation of the species on the electrode, could be clearly evaluated from the AFM images. Results indicated that the fluctuation decreased gradually along with the hydrolysis time of TEOS in the step of *in situ* growth of SiO_2 gel. Bare BDD had a fluctuation about 170 nm (image not given). After 10 min hydrolysis at 50 °C, the fluctuation reduced to 120 nm (image not shown), indicating that the lower part of the BDD surface was filled by SiO_2 gel. When the hydrolysis time was extended to 30 min, fluctuation of 70 nm was observed, implying that the BDD surface was well covered by SiO_2 gel (Fig. 2a). SEM image of SiO_2/BDD profile (Fig. 2c) also provided obvious evidence that a SiO_2 gel layer was *in situ* fabricated on the BDD surface. The fluctuation of morphology would be only 20 nm if hydrolysis time was increased to 120 min (image not shown). When Cyt *c* was immobilized on the SiO_2/BDD, the fluctuation of the resultant Cyt *c*/SiO_2/BDD decreased ulteriorly (Fig. 2b), but obvious change of the surface morphology well proved the successful immobilization of Cyt *c*.

Fig. 3 shows the XRD patterns of bare BDD and SiO_2 gel covered BDD. There were two sharp peaks in the response of bare BDD in 2θ values of 28° and 44°, corresponding to the Si substrate and diamond (111), respectively. When SiO_2 gel was fabricated on the BDD substrate, there was a wide peak that appeared at 2θ values between 20° and 30°, which attributed to the amorphous SiO_2 generated from hydrolysis of TEOS vapor.

3.3. Biocompatibility and bioactivity maintenance ability study

Biocompatibility of SiO_2 gel was estimated by UV–vis absorption spectra. The Soret absorption band of Cyt *c* was known at about 410 nm (Fig. 4a). Fig. 4b was recorded by directly casting Cyt *c* PBS (pH 6.86) onto a glass sheet. It could be seen that the peak shape became much broader. However, the situation was different when Cyt *c* molecule was immobilized on the SiO_2 gel matrix. The peak was well shaped and no shift was observed (Fig. 4c). This implied that the SiO_2 gel matrix had good biocompatibility and was helpful for the Cyt *c* molecule to maintain its native conformation and bioactivity.

Proteins often denature in high or low pH, which greatly limits the application of biosensors. Therefore, influence of pH to Cyt *c* activity was investigated as following: sandwich/BDD was dipped in a series of PBS (pH 3–12) for 30 min, respectively; then it was taken out and incubated in pH 7 PBS for 5 min. Then CV was performed. As shown in Fig. 5a, formal potential shifted negatively along with increase of pH. A linear relationship was obtained between the formal potential and pH, suggesting that the electrochemistry of Cyt *c* involved a proton process. Under extreme pH, the

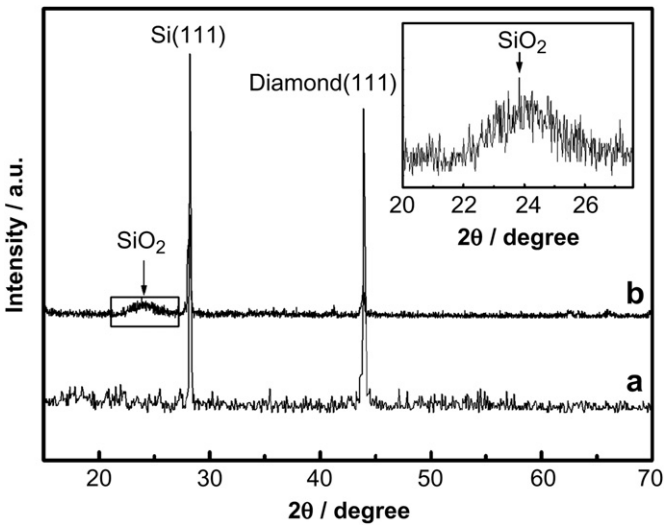

Fig. 3. The XRD patterns for bare BDD (a) and SiO_2/BDD (b).

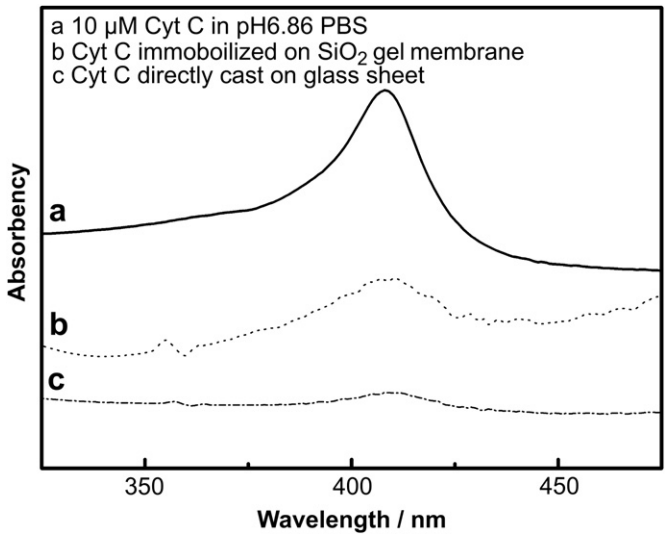

Fig. 4. The UV–vis absorption spectra for (a) 10 μM Cyt *c* in pH 6.86 PBS; (b) Cyt *c* directly cast on glass sheet and (c) Cyt *c* immobilized on SiO_2 gel membrane.

shape of redox peaks was not so symmetrical. But when the electrode was incubated in pH 7 solution, the redox peaks became symmetrical again (see Fig. 5b) which indicated that Cyt *c* did not denaturalize irreversibly. The result showed that the sandwich structure could remarkably restrain the denaturation of the protein in extreme pH. This resulted from the rigidity of SiO_2, which didn't allow the protein to undergo denaturing unfolding motion [52], or the pH of internal film was different from that in bulk solution [53]. The SiO_2 gel was hence conceived to be "semi-open", which permitted the communication between immobilized Cyt *c* and the ions in solution, and simultaneously, well shielding Cyt *c* from extreme outer environment.

EIS was carried out to investigate the changes of electron transfer resistance (Ret) that aroused from every surface modification step. Fig. 6 shows the curves of different electrodes. Ret can be directly measured as the semicircle diameter [54]. As shown in Fig. 6, Ret of SiO_2/BDD dramatically increased compared with bare BDD, suggesting that SiO_2 gel membrane was successfully fabricated. After further immobilization of Cyt *c*, it decreased, since the anion in PBS approached the attached Cyt c (pI 10.5, positively charged in neutral medium) easily, which was also an evidence of successful immobilization of Cyt *c*, similar to the previous reports [2]. If another layer of SiO_2 was constructed continually, Ret increased again, but still smaller than that of SiO_2/BDD, implying that the electron transfer tunnel was successfully constructed.

3.4. Direct electrochemistry behavior of immobilized Cyt c on sandwich/BDD

The electrochemical behavior of Cyt *c* immobilized between the SiO_2 gel interlayer in PBS (pH 6.86) was investigated by CV. A pair of well shaped redox peaks were observed at about −0.036 V (vs. SCE, Fig. 7a), characteristic of the Cyt *c* heme Fe^{III}/Fe^{II} redox couples, which could not be observed on either bare BDD (Fig. 7a, dotted curve 1) or SiO_2/BDD electrode (Fig. 7a, dotted curve 2). It could be seen that the CVs of SiO_2/Cyt *c*/SiO_2/BDD electrode were almost symmetrical and the redox peak currents increased linearly with the scan rates between 0.1 and 0.5 V s^{-1} (Fig. 7b), suggesting that electrode reactions were typical of the surface-controlled processes. The value of the electron transfer rate constant (k_s) was 1.39 s^{-1}, which could be estimated according to Laviron [55]. It was much higher than that of Cyt *c* adsorbed on mesoporous niobium

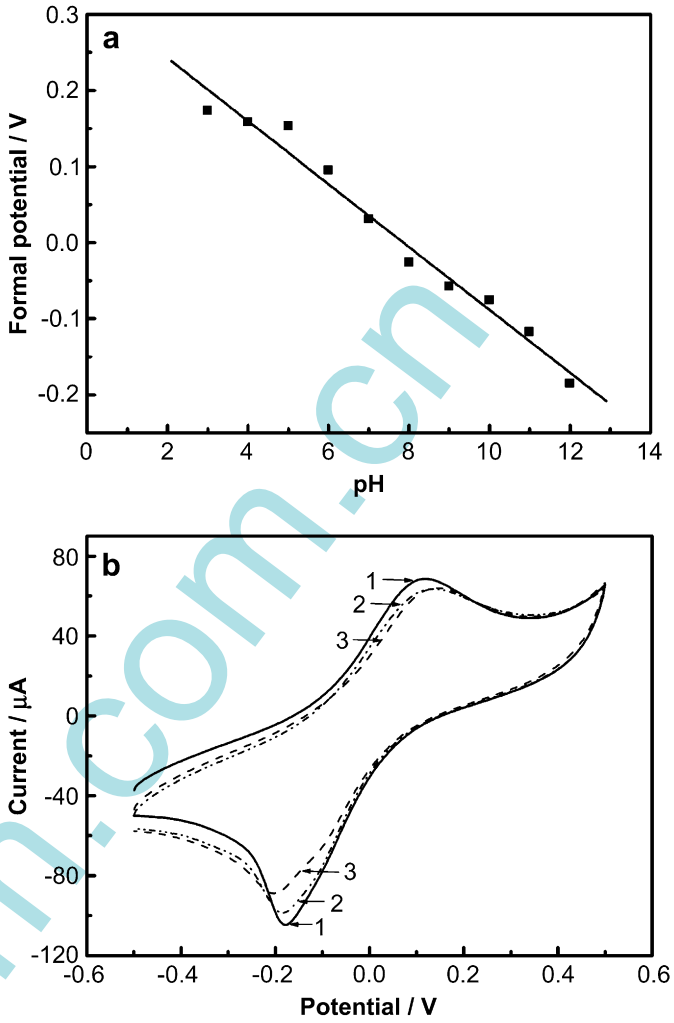

Fig. 5. (a) The formal potential shift of the SiO_2/Cyt *c*/SiO_2/BDD electrode along with the pH of PBS; (b) CVs of the SiO_2/Cyt *c*/SiO_2/BDD electrode in pH 7 PBS directly (1) and after dipped in pH 12 PBS for 30 min (2) and after dipped in pH 3 PBS for 30 min (3) and then incubated in pH 7 PBS for 5 min.

oxide film/ITO (0.28 s^{-1}) [56] and NaY zeolite/GCE (0.78 ± 0.04 s^{-1}) [57], slightly higher than that on colloidal Au/carbon paste (1.21 ± 0.08 s^{-1}) [58], and L-cysteine/Au (1.25 ± 0.10 s^{-1}) [40]. This faster electron transfer rate indicated that SiO_2 gel was an excellent promoter for the electron transfer between Cyt *c* and the BDD base, and meanwhile, a good matrix for the immobilization of Cyt *c*.

According to Laviron's equation [59]: $I_p = n^2F^2vA\Gamma/4RT$, the average surface coverage of Cyt *c* adsorbed on the electrode was 2.22×10^{-9} mol/cm^2, higher than monolayer adsorption. This was due to the good immobilization ability of SiO_2 gel to biomolecule.

3.5. Biocatalytic oxidative property to nitrite

Two anodic peaks on the sandwich electrode were observed at 0.06 V (peak I) and 0.6 V (peak II), respectively, when studied by DPV in pH 6.86 PBS, as shown in Fig. 8, curve 1. More attractively, when 0.5 mM $NaNO_2$ was added into the bulk solution, another anodic peak appeared at 0.7 V (Fig. 8, curve 2, peak III); while this peak didn't appear on SiO_2/BDD electrode. The peak current increased along with the $NaNO_2$ concentation (Fig. 8, curves 3 and 4). This peak was herein attributed to the interaction between Cyt *c* and nitrite.

According to literatures [60], heme proteins can be oxidized into oxoiron(IV) proteins and oxoiron(IV) proteins π-cation radicals via

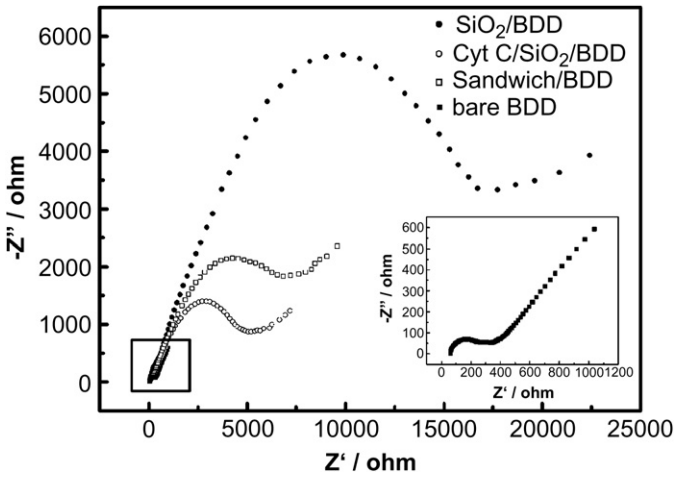

Fig. 6. The EIS patterns of different electrodes.

one-electron and two-electron oxidation by chemical oxidants or direct electrochemical oxidation [41,61]. Here we suggested that peak II was attributed to the further oxidation of Cyt *c*, and the product could catalyse the oxidation of nitrite, which resulted in

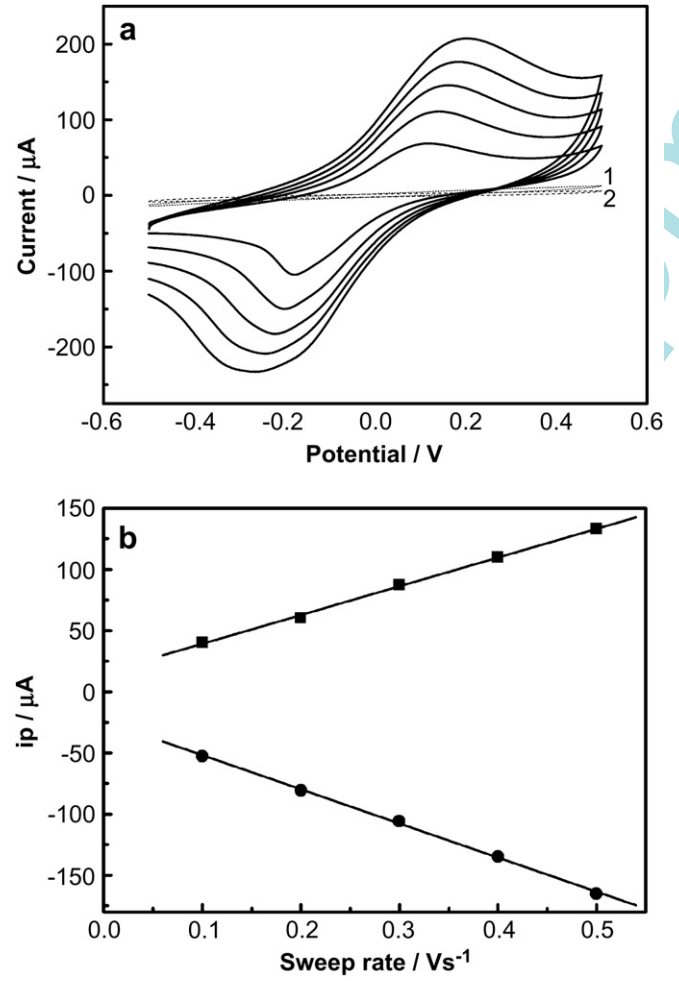

Fig. 7. (a) CVs of the SiO_2/Cyt *c*/SiO_2/BDD electrode (solid curves) at different scan rates (from inner to outer: 0.1, 0.2, 0.3, 0.4 and 0.5 V s^{-1}, respectively) and bare BDD electrode (dotted curve, 1) and SiO_2/BDD electrode (dotted curve, 2) at 0.1 V s^{-1} in 25 mM PBS (pH 6.86); (b) the plot of cathodic (●) and anodic (■) currents versus scan rate of the SiO_2/Cyt *c*/SiO_2/BDD electrode.

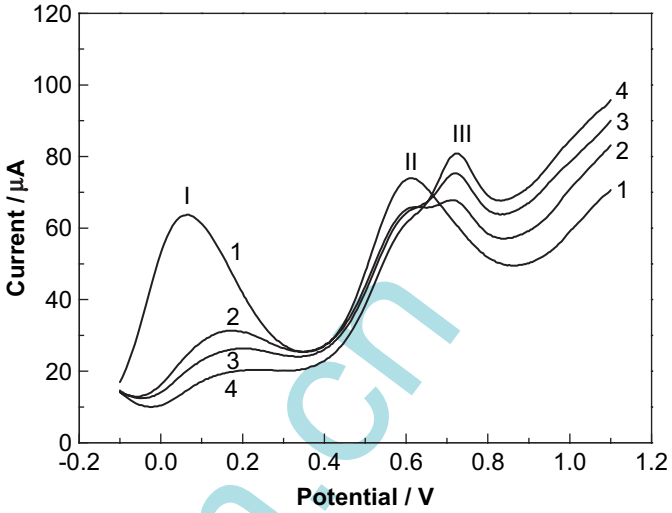

Fig. 8. DPVs of SiO_2/Cyt *c*/SiO_2/BDD electrode in 25 mM PBS containing 0 (1), 0.5 (2), 0.75 (3) and 1.0 mM (4) $NaNO_2$.

the peak III. A possible mechanism was accordingly proposed. As reported, NO_2^- could be oxidized by heme peroxidases in the presence of H_2O_2 [62,63], since these heme proteins could be chemically peroxidized to highly active protein π-cation. Lei and coworkers [61] studied the oxidative reaction of NO and NO_2^- catalyzed by iron porphyrin, which was well known as the electroactive center of Cyt *c*. Results showed that iron porphyrin could be oxidized to oxoiron and π-cation by stepwise direct oxidation, but only π-cation could interact with nitrite while oxoiron just selectively oxidized NO. As shown in Fig. 8, peak I was attributed to the oxidation of ferrous Cyt *c* to ferric form, corresponding to reaction I listed in Scheme 2. Further oxidation product must be Cyt *c* π-cation since it could interact with NO_2^-. There was only one anodic peak, which might be because the ferric Cyt *c* could be oxidized to Cyt *c* π-cation by one-step direct electrochemistry oxidation, reaction II in Scheme 2, similar to H_2O_2 to heme peroxidase. This might be in virtue of the outstanding properties of BDD substrate, on which the generation of Cyt *c* π-cation was easier. Nitrogen dioxide radical ($\bullet NO_2$) and oxoiron Cyt *c* were considered to be the intermediate and they could further interact, with NO_3^- and ferric Cyt *c* as the product. Reaction III in Scheme 2 describes the two-step interaction.

The biocatalytic oxidation property of Cyt *c* π-cation to nitrite brought the possibility to detect nitrite in solution. Fig. 9 shows the variation of current with time obtained at the SiO_2/Cyt *c*/SiO_2/BDD electrode, with the operating potential of 0.7 V (vs. SCE). The oxidation current was proportional to the concentration of nitrite in the range of 1.0×10^{-6}–1.0×10^{-3} M, and the detection limit was 0.5 μM at S/N of 3, with a sensitivity of 0.17 μA μM^{-1} cm^{-2}. It is notable that this detection limit is obviously lower than the results obtained at some nitrite biosensors such as Hb/colloidal gold nanoparticles/TiO_2 sol–gel film modified GCE [36] or Mb–ZnO-modified GE [64], and comparable or lower than detection limits obtained with other electrochemical methods such as lead(IV) oxide–graphite composite electrodes (0.9 μM) [31] and manganese dioxide–graphite composite electrodes (0.4 μM) [32], indicating that the fabricated sandwich structured biosensor can potentially be used for monitoring of the concentration of nitrite sensitively.

The sandwich electrode exhibited high stability. It showed no fading for voltammetric current when cycled between −0.5 and 0.5 V (vs. SCE) in PBS (pH 6.86) for 50 times. When stored in PBS (pH 6.86) at 4 °C, the current response almost stabilized for at least one week. Even after long time dip in strong acidic or alkaline

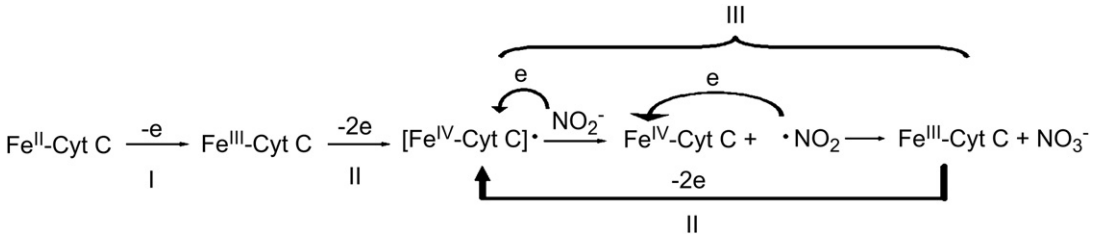

Scheme 2. The reaction mechanisms for Cyt *c* and nitrite.

solution (pH 3 or pH 12), the sensitivity was retained. In addition, no obvious fading in response to NO_2^- was observed after 30 days. The preparation of seven electrodes with the same method showed an acceptable reproducibility, with a RSD of 5.6% for the current determined at 50 μM NO_2^-. The good stability and repeatability resulted from the sandwich structure, which protected the biomolecule against dry and severe environment. On the other hand, the mass transfer was guaranteed between inner Cyt *c* and outer bulk electrolyte through the "semi-open" SiO_2 gel membrane, which ensured the sensitive response. The good maintenance of bioactivity of Cyt *c* could be attributed to the outstanding properties of BDD substrate and the novel sandwich structure. Therefore, it opened a hopeful prospect for designing an oxidative amperometric biosensor to nitrite. Meanwhile, its high stability and sensitivity effectively made the biosensor display a reasonable longer using-life and more determination times, which would greatly reduce its one-time using cost, indicating prospective economical and practical significance.

4. Conclusions

In this study, SiO_2/Cyt *c*/SiO_2 sandwich structure was designed and constructed. With a simple surface vapor sol–gel method, SiO_2 gel membrane was fabricated on the pretreated BDD electrode. The growth rate of SiO_2 gel was accelerated evidently by optimization of the temperature and the pH values of the hydrolysis solution in the surface vapor sol–gel process. Cyt *c* was immobilized between the SiO_2 gel membranes through electrostatic attraction via carefully controlling the pH of the solution. The bioactivity of Cyt *c* was retained well by the sandwich structure. Meanwhile, it was proved that the sandwich was semi-opened. This structure had two significant advantages: permitted the communication between biomolecule and bulk solution, and protected the biomolecule from the influence of extreme environment. Cyt *c* immobilized in the sandwich structure not only exhibited good direct electrochemistry, but also could be oxidized to Cyt *c* π-cation, a strong oxidant which could oxidize NO_2^- to NO_3^-. A possible mechanism was proposed to this electrocatalytic oxidation reaction. The ferrous Cyt *c* was directly oxidized to Cyt *c* π-cation by two direct electrochemistry steps; while the Cyt *c* π-cation was highly reactive and could oxidize nitrite to nitrate through a two-step reaction. Electrochemical experiments indicated that the response signal increased along with the concentration of nitrite. Thus an oxidative amperometric biosensor to nitrite with satisfactory linear range and detection limit was proposed for the first time. A facile and simple way to immobilize biomolecule was thus provided and a promising prospect was hence opened for designing oxidative nitrite biosensor.

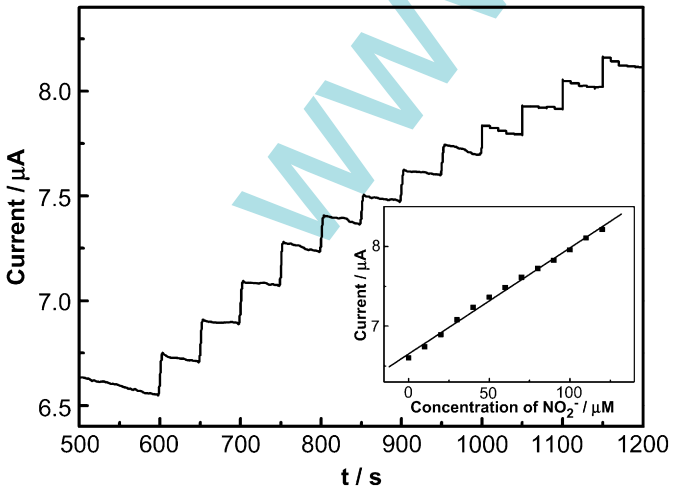

Fig. 9. Typical current–time plot for successive additions of 10 μM $NaNO_2$ on the SiO_2/Cyt *c*/SiO_2/BDD electrode. The inset is the relationship between the current and corresponding concentration of $NaNO_2$.

Acknowledgements

This research is supported by the National Natural Science Foundation of China (No. 20577035, 50478106), Nanometer Science Foundation of Shanghai, China (No. 0652nm030), 863 Program (Project NO.2008AA06Z329) from the Ministry of Science, Shanghai Educational Development Foundation (No. 2007CG24) and Program for Young Excellent Talents in Tongji University (No. 2006kj060).

References

[1] Wang J, Li M, Shi Z, Li N, Gu Z. Direct electrochemistry of cytochrome *c* at a glassy carbon electrode modified with single-wall carbon nanotubes. Anal Chem 2002;74:1993–7.
[2] Zhao GC, Yin ZZ, Zhang L, Wei XW. Direct electrochemistry of cytochrome *c* on a multi-walled carbon nanotubes modified electrode and its electrocatalytic activity for the reduction of H_2O_2. Electrochem Commun 2005;7:256–60.
[3] Jiang X, Zhang L, Dong S. Assemble of poly(aniline-*co*-*o*-aminobenzenesulfonic acid) three-dimensional tubal net-works onto ITO electrode and its application for the direct electrochemistry and electrocatalytic behavior of cytochrome *c*. Electrochem Commun 2006;8:1137–41.
[4] Lawrence NS, Deo RP, Wang J. Biocatalytic carbon paste sensors based on a mediator pasting liquid. Anal Chem 2004;76:3735–9.
[5] Yamamoto K, Ohgaru T, Torimura M, Kinoshita H, Kano K, Ikeda T. Highly-sensitive flow injection determination of hydrogen peroxide with a peroxidase-immobilized electrode and its application to clinical chemistry. Anal Chim Acta 2000;406:201–7.
[6] Polsky R, Harper JC, Dirk SM, Arange DC, Wheeler DR, Brozik SM. Diazonium-functionalized horseradish peroxidase immobilized via addressable electrodeposition: direct electron transfer and electrochemical detection. Langmuir 2007;23:364–6.
[7] Zhou YL, Zhi JF. Development of an amperometric biosensor based on covalent immobilization of tyrosinase on a boron-doped diamond electrode. Electrochem Commun 2006;8:1811–6.
[8] Lojou É, Bianco P. Membrane electrodes for protein and enzyme electrochemistry. Electroanalysis 2004;16:1113–22.
[9] Muguruma H, Kase Y, Uehara H. Nanothin ferrocene film plasma polymerized over physisorbed glucose oxidase: high-throughput fabrication of bioelectronic devices without chemical modifications. Anal Chem 2005;77:6557–62.

[10] Dai Z, Xu X, Ju H. Direct electrochemistry and electrocatalysis of myoglobin immobilized on a hexagonal mesoporous silica matrix. Anal Biochem 2004; 332:23–31.
[11] Chen H, Wang Y, Dong S, Wang E. Direct electrochemistry of cytochrome *c* at gold electrode modified with fumed silica. Electroanalysis 2005;17:1801–5.
[12] He P, Hu N, Rusling JF. Driving forces for layer-by-layer self-assembly of films of SiO_2 nanoparticles and heme proteins. Langmuir 2004;20:722–9.
[13] Liu H, Rusling JF, Hu N. Electroactive core–shell nanocluster films of heme proteins, polyelectrolytes, and silica nanoparticles. Langmuir 2004;20: 10700–5.
[14] Kamau GN, Guto MP, Munge B, Panchagnula V, Rusling JF. Myoglobin coadsorbed on electrodes from microemulsions provides reversible electrochemistry and tunable electrochemical catalysis. Langmuir 2003;19: 6979–81.
[15] Wu Y, Hu S. The fabrication of a colloidal gold–carbon nanotubes composite film on a gold electrode and its application for the determination of cytochrome *c*. Colloid Surf B 2005;41:299–304.
[16] Xu J, Granger MC, Chen Q, Strojek JW, Lister TE, Swain GM. Boron-doped diamond thin-film electrodes. Anal Chem News Features 1997;69:591A–7.
[17] Granger MC, Witek M, Xu J, Wang J, Hupert M, Hanks A, et al. Standard electrochemical behavior of high-quality, boron-doped polycrystalline diamond thin-film electrodes. Anal Chem 2000;72:3793–804.
[18] Ferro S, Battisti AD. Electron transfer reactions at conductive diamond electrodes. Electrochim Acta 2002;47:1641–9.
[19] Hupert M, Muck A, Wang J, Stotter J, Cvackova Z, Haymond S, et al. Conductive diamond thin-films in electrochemistry. Diamond Relat Mater 2003; 12:1940–9.
[20] Soh KL, Kang WP, Davidson JL, Wong YM, Wisitsora-At A, Swain G, et al. CVD diamond anisotropic film as electrode for electrochemical sensing. Sensor Actuat B 2003;91:39–45.
[21] Zhang J, Oyama M. Electroanalysis of myoglobin and hemoglobin with a boron-doped diamond electrode. Microchem J 2004;78:217–22.
[22] Rao TN, Loo BH, Sarada BV, Terashima C, Fujishima A. Electrochemical detection of carbamate pesticides at conductive diamond electrodes. Anal Chem 2002;74:1578–83.
[23] Zhi JF, Wang HB, Nakashima T, Rao TN, Fujishima A. Electrochemical incineration of organic pollutants on boron-doped diamond electrode. Evidence for direct electrochemical oxidation pathway. J Phys Chem B 2003; 107:13389–95.
[24] Terashima C, Rao TN, Sarada BV, Tryk DA, Fujishima A. Electrochemical oxidation of chlorophenols at a boron-doped diamond electrode and their determination by high-performance liquid chromatography with amperometric detection. Anal Chem 2002;74:895–902.
[25] Sarada BV, Rao TN, Tryk DA, Fujishima A. Electrochemical oxidation of histamine and serotonin at highly boron-doped diamond electrodes. Anal Chem 2000;72:1632–8.
[26] Rao TN, Yagi I, Miwa YT, Tryk DA, Fujishima A. Electrochemical oxidation of NADH at highly boron-doped diamond electrodes. Anal Chem 1999;71: 2506–11.
[27] Ivandini TA, Rao TN, Fujishima A, Einaga Y. Electrochemical oxidation of oxalic acid at highly boron-doped diamond electrodes. Anal Chem 2006;78:3467–71.
[28] Compton RG, Foord JS, Marken F. Electroanalysis at diamond-like and doped-diamond electrodes. Electroanalysis 2003;15:1349–63.
[29] Moorcroft MJ, Davis J, Compton RG. Detection and determination of nitrate and nitrite: a review. Talanta 2001;54:785–803.
[30] Šljukić B, Banks CE, Crossley A, Compton RG. Copper oxide–graphite composite electrodes: application to nitrite sensing. Electroanalysis 2007;19:79–84.
[31] Šljukić B, Banks CE, Crossley A, Compton RG. Lead(IV) oxide–graphite composite electrodes: application to sensing of ammonia, nitrite and phenols. Anal Chim Acta 2007;587:240–6.
[32] Langley CE, Šljukić B, Banks CE, Compton RG. Manganese dioxide graphite composite electrodes: application to the electroanalysis of hydrogen peroxide, ascorbic acid and nitrite. Anal Sci 2007;23:165–70.
[33] Davis J, Moorcroft MJ, Wilkins SJ, Compton RG, Cardosi MF. Electrochemical detection of nitrate and nitrite at a copper modified electrode. Analyst 2000; 125:737–42.
[34] Davis J, Compton RG. Sonoelectrochemically enhanced nitrite detection. Anal Chim Acta 2000;404:241–7.
[35] Wu Q, Storrier GD, Parients F, Wang Y, Shapleigh JP, Abruña HD. A nitrite biosensor based on a maltose binding protein nitrite reductase fusion immobilized on an electropolymerized film of a pyrrole-derived bipyridinium. Anal Chem 1997;69:4856–63.
[36] Yang W, Bai Y, Li Y, Sun C. Amperometric nitrite sensor based on hemoglobin/colloidal gold nanoparticles immobilized on a glassy carbon electrode by a titania sol–gel film. Anal Bioanal Chem 2005;382:44–50.
[37] Li M, He P, Zhang Y, Hu N. An electrochemical investigation of hemoglobin and catalase incorporated in collagen films. Biochim Biophys Acta 2005;1749:43–51.
[38] Yao H, Li N, Xu JZ, Zhu JJ. Direct electrochemistry and electrocatalysis of hemoglobin in gelatine film modified glassy carbon electrode. Talanta 2007; 71:550–4.
[39] Astier Y, Canters GW, Davis JJ, Hill HAO, Verbeet MP, Wijma HJ. Sensing nitrite through a pseudoazurin-nitrite reductase electron transfer relay. Chemphyschem 2005;6:1114–20.
[40] Liu YC, Cui SQ, Zhao J, Yang ZS. Direct electrochemistry behavior of cytochrome *c*/L-cysteine modified electrode and its electrocatalytic oxidation to nitric oxide. Electrochem 2006;71:121–5.
[41] Chen SM, Chen SV. The bioelectrocatalytic properties of cytochrome *c* by direct electrochemistry on DNA film modified electrode. Electorchim Acta 2003;48: 513–29.
[42] Yamada S, Suruga K, Ogawa M, Hama T, Satoh T, Kawachi R, et al. Appearance of nitrite reducing activity of cytochrome *c* upon heat denaturation. Biosci Biotech Bioch 2002;66:2044–51.
[43] Suruga K, Nagasawa N, Yamada S, Satoh T, Kawachi R, Nishio T, et al. Radiation-induced enhancement of nitrite reducing activity of cytochrome c. J Agric Food Chem 2003;51:6835–43.
[44] Castro L, Eiserich JP, Sweeney S, Radi R, Freeman BA. Cytochrome *c*: a catalyst and target of nitrite-hydrogen peroxide-dependent protein nitration. Arch Biochem Biophys 2004;421:99–107.
[45] Deng H. Nitrite anions induce nitrosative deamination of peptides and proteins. Rapid Commun Mass Spectrom 2006;20:3634–8.
[46] Yutaka O, Hideo S. Reaction of cytochrome *c* with nitrite and nitric oxide. A model of dissimilatory nitrite reductase. J Biochem 1978;84:1543–52.
[47] Rao TN, Ivandini TA, Terashima C, Sarada BV, Fujishima A. Applications of bare and modified diamond electrodes in electroanalysis. New Diam Front C Tec 2003;12:79–88.
[48] Marken F, Paddon CA, Asogan D. Direct cytochrome *c* electrochemistry at boron-doped diamond electrodes. Electrochem Commun 2002;4:62–6.
[49] Shi G, Sun Z, Liu M, Zhang L, Liu Y, Qu Y, et al. Electrochemistry and electrocatalytic properties of hemoglobin in layer-by-layer films of SiO_2 with vapor–surface sol–gel deposition. Anal Chem 2007;79:3581–9.
[50] Guo W, Lu H, Hu N. Comparative bioelectrochemical study of two types of myoglobin layer-by-layer films with alumina: vapor–surface sol–gel deposited Al_2O_3 films versus Al_2O_3 nanoparticle films. Electrochim Acta 2006;52: 123–32.
[51] Lu H, Yang J, Rusling JF, Hu N. Vapor–surface sol–gel deposition of titania alternated with protein adsorption for assembly of electroactive, enzyme-active films. Electroanalysis 2006;18:379–90.
[52] Jin W, Brennan JD. Properties and applications of proteins encapsulated within sol–gel derived materials. Anal Chim Acta 2002;461:1–36.
[53] Panchagnula V, Kumar CV, Rusling JF. Ultrathin layered myoglobin–polyion films functional and stable at acidic pH Values. J Am Chem Soc 2002;124: 12515–22.
[54] Gu H, Su XD, Loh KP. Electrochemical impedance sensing of DNA hybridization on conducting polymer film-modified diamond. J Phys Chem B 2005;109: 13611–8.
[55] Laviron E. General expression of the linear potential sweep voltammogram in the case of diffusionless electrochemical systems. J Electroanal Chem 1979; 101:19–28.
[56] Xu X, Tian B, Kong J, Zhang S, Liu B, Zhao D. Ordered mesoporous niobium oxide film: a novel matrix for assembling functional proteins for bioelectrochemical applications. Adv Mater 2003;15:1932–7.
[57] Dai Z, Liu S, Ju H. Direct electron transfer of cytochrome *c* immobilized on a NaY zeolite matrix and its application in biosensing. Electrochim Acta 2004; 49:2139–44.
[58] Ju H, Liu S, Ge B, Lisdat F, Scheller FW. Electrochemistry of cytochrome *c* immobilized on colloidal gold modified carbon paste electrodes and its electrocatalytic activity. Electroanalysis 2002;14:141–7.
[59] Laviron E. The use of linear potential sweep voltammetry and of a.c. voltammetry for the study of the surface electrochemical reaction of strongly adsorbed systems and of redox modified electrodes. J Electroanal Chem 1979; 100:263–70.
[60] Everse J, Hsia N. The toxicities of native and modified hemoglobins. Free Radical Biol Med 1997;22:1075–99.
[61] Lei J, Ju H, Ikeda O. Catalytic oxidation of nitric oxide and nitrite mediated by water-soluble high-valent iron porphyrins at an ITO electrode. J Electroanal Chem 2004;567:331–8.
[62] Shibata H, Kono Y, Yamashita S, Sawa Y, Ochiai H, Tanaka K. Degradation of chlorophyll by nitrogen dioxide generated from nitrite by the peroxidase reaction. Biochim Biophys Acta 1995;1230:45–50.
[63] Viliet AVD, Eiserich JP, Halliwell B, Cross CE. Formation of reactive nitrogen species during peroxidase-catalyzed oxidation of nitrite. J Biol Chem 1997; 272:7617–25.
[64] Zhao G, Xu JJ, Chen HY. Interfacing myoglobin to graphite electrode with an electrodeposited nanoporous ZnO film. Anal Biochem 2006;350:145–50.